

Meson Decay Constants from the Valence Approximation  
to Lattice QCD

F. Butler, H. Chen, J. Sexton<sup>1</sup>, A. Vaccarino,  
and D. Weingarten  
IBM Research  
P.O. Box 218, Yorktown Heights, NY 10598

ABSTRACT

We evaluate  $f_\pi/m_\rho$ ,  $f_K/m_\rho$ ,  $1/f_\rho$ , and  $m_\phi/(f_\phi m_\rho)$ , extrapolated to physical quark mass, zero lattice spacing and infinite volume, for lattice QCD with Wilson quarks in the valence (quenched) approximation. The predicted ratios differ from experiment by amounts ranging from 12% to 17% equivalent to between 0.9 and 2.8 times the corresponding statistical uncertainties.

---

<sup>1</sup>permanent address: Department of Mathematics, Trinity College, Dublin 2, Republic of Ireland

## 1 INTRODUCTION

In a recent paper [1] we presented lattice QCD predictions for the masses of eight low-lying hadrons, extrapolated to physical quark mass, zero lattice spacing, and infinite volume, using Wilson quarks in the valence (quenched) approximation. The masses we found were within 6% of experiment, and all differences between prediction and experiment were consistent with the calculation's statistical uncertainty. We argued that this result could be interpreted as quantitative confirmation of the low-lying mass predictions both of QCD and of the valence approximation. It appeared to us unlikely that eight different valence approximation masses would agree with experiment yet differ significantly from QCD's predictions including the full effect of quark-antiquark vacuum polarization.

We have now evaluated the infinite volume, zero lattice spacing, physical quark mass limit of  $f_\pi/m_\rho$ ,  $f_K/m_\rho$ ,  $1/f_\rho$ , and  $m_\phi/(f_\phi m_\rho)$ . To our knowledge there have been no previous systematic calculations of this physical limit of lattice meson decay constants. A review of earlier work is given in Ref. [2]. The predicted  $m_\phi/(f_\phi m_\rho)$  lies above its observed value by about its statistical uncertainty of approximately 15%. The predicted  $f_\pi/m_\rho$  and  $1/f_\rho$  are close to 12% below experiment, equivalent to about 0.9 times the corresponding statistical uncertainties, and  $f_K/m_\rho$  is below experiment by 17%, equal to 2.8 times its statistical uncertainty.

Although overall the predicted values could be considered in fair agreement with experiment, the result that three of four decay constants range from 0.9 to 2.8 standard deviations below experiment suggests the possibility that the true, underlying values, if determined without statistical uncertainties, would fall somewhat below experiment. One possible source of such disagreement is that we have assumed exact isospin symmetry and ignored electromagnetic effects. In particular, although our prediction for  $f_\pi$  lies below measured values determined from charged pion decays, reported numbers for the neutral pion decay constant [3] are quite close to our result. The significance of the closer agreement between our predicted  $f_\pi$  and the neutral pion decay constant is unclear to us, however, as a consequence of the systematic uncertainties arising in the experimental determination of the neutral pion decay

constant.

Another possible source of disagreement between our numbers and experiment may be the valence approximation itself. A simple physical argument tends to support of this alternative [4]. The valence approximation may be viewed as replacing the momentum and frequency dependent color dielectric constant arising from quark-antiquark vacuum polarization with its low momentum limit [5]. At low momentum, then, the effective quark charge appearing in the valence approximation will agree with the low momentum effective charge of the full theory. The valence approximation might thus be expected to be fairly reliable for low-lying baryon and meson masses, which are determined largely by the long distance behavior of the chromoelectric field. The valence approximation's effective quark charge at higher momentum can be obtained from the low momentum charge by the Callan-Symanzik equation. As a consequence of the absence of dynamical quark-antiquark vacuum polarization, the quark charge in the valence approximation will fall faster with momentum than it does in the full theory, at short distance the attractive quark-antiquark potential in the valence approximation will be weaker than in the full theory, and meson wave functions in the valence approximation will be pulled into the origin less than in the full theory. Since decay constants are proportional to the square of wave functions at the origin, decay constants in the valence approximation could be expected to be smaller than in the full theory.

The calculations described here were done on the GF11 parallel computer at IBM Research [6] and use the same collection of gauge configurations and quark propagators generated for the mass calculations of Ref. [1]. The full set of mass and decay constant calculations took approximately one year to complete. GF11 was used in configurations ranging from 384 to 480 processors, with sustained speeds ranging from 5 Gflops to 7 Gflops. With the present set of improved algorithms and 480 processors, these calculations could be repeated in less than four months.

## 2 DEFINITIONS

The normalization we adopt for pseudoscalar and vector decay constants in continuum QCD is

$$\begin{aligned} \langle 0 | J_j^\mu(0) | V(p, \epsilon, j) \rangle &= \epsilon^\mu m_j F_j, \\ \langle 0 | J_j^{5\mu}(0) | P(p, j) \rangle &= p^\mu f_j, \end{aligned}$$

for vector and pseudoscalar states,  $|V(p, \epsilon, j)\rangle$  and  $|P(p, j)\rangle$ , respectively, normalized by

$$\langle p | q \rangle = (2\pi)^3 p^0 \delta(\vec{p} - \vec{q}).$$

Here  $j$  is a flavor-SU(3) octet index and vector and axial vector flavor-SU(3) currents  $J_j^\mu(x)$  and  $J_j^{5\mu}(x)$  are related to canonical continuum quark and antiquark fields,  $\bar{\psi}_c$  and  $\psi_c$ , and an orthonormal set of flavor-SU(3) matrices  $\lambda_j$  by

$$\begin{aligned} J_j^\mu(x) &= \bar{\psi}_c(x) \gamma^\mu \lambda_j \psi_c(x), \\ J_j^{5\mu}(x) &= \bar{\psi}_c(x) \gamma^5 \gamma^\mu \lambda_j \psi_c(x), \\ \text{tr}(\lambda_j \lambda_j) &= \frac{1}{2}. \end{aligned}$$

Assuming exact isospin symmetry, we have

$$\begin{aligned} f_i &= f_\pi & i &= 1, \dots, 3, \\ f_i &= f_K & i &= 4, \dots, 7, \\ F_i &= \frac{m_\rho}{f_\rho} & i &= 1, \dots, 3. \end{aligned}$$

In the valence approximation we have, in addition,

$$F_8 = \frac{3m_\phi}{\sqrt{2}f_\phi}.$$

For simplicity, we will also use the names  $F_\rho$  and  $F_\phi$  for  $F_1$  and  $F_8$ , respectively. Our normalization gives  $f_\pi$  the value  $(93.15 \pm 0.11)$  MeV.

The hadron mass calculation of Ref. [1] was done using gaussian smeared lattice quark and antiquark fields defined in Coulomb gauge. Smeared fields have,

therefore, also been adopted for the present calculation. The smeared field  $\phi_r(\vec{x}, t)$  is related by the lattice antiquark field  $\psi_\ell(\vec{x}, t)$  by

$$\begin{aligned}\phi_r(\vec{x}, t) &= \sum_{\vec{y}} G_r(\vec{x} - \vec{y}) \psi_\ell(\vec{y}, t), \\ G_r(\vec{z}) &= (\sqrt{\pi r})^{-3} \exp(-\frac{|\vec{z}|^2}{r^2}).\end{aligned}$$

The field  $\bar{\phi}_r(\vec{x}, t)$  is defined correspondingly from  $\bar{\psi}_\ell(\vec{x}, t)$ . We take the smeared fields  $\phi_0(x)$  and  $\bar{\phi}_0(x)$  to be  $\psi(x)$  and  $\bar{\psi}(x)$ , respectively. From these fields, define smeared currents by

$$\begin{aligned}J_{jr}^5(x) &= \bar{\phi}_r(x) \gamma^5 \lambda_j \phi_r(x), \\ J_{jr}^\mu(x) &= \bar{\phi}_r(x) \gamma^\mu \lambda_j \phi_r(x), \\ J_{jr}^{5\mu}(x) &= \bar{\phi}_r(x) \gamma^5 \gamma^\mu \lambda_j \phi_r(x).\end{aligned}$$

Define the correlation functions  $C_{jr'r}^P(t)$ ,  $C_{jr'r}^V(t)$  and  $C_{jr'r}^A(t)$  to be

$$C_{jr'r}^P(t) = \sum_{\vec{x}} \langle [J_{jr'}^5(\vec{x}, t)]^\dagger J_{jr}^5(0, 0) \rangle, \quad (2.1)$$

$$C_{jr'r}^V(t) = \sum_{\vec{x}} \langle [J_{jr'}^i(\vec{x}, t)]^\dagger J_{jr}^i(0, 0) \rangle, \quad (2.2)$$

$$C_{jr'r}^A(t) = \sum_{\vec{x}} \langle [J_{jr'}^{50}(\vec{x}, t)]^\dagger J_{jr}^{50}(0, 0) \rangle. \quad (2.3)$$

Then for a set of constants  $Z_{jr'r}^P$ ,  $Z_{jr'r}^V$  and  $Z_{jr'r}^A$ , these correlation functions have the asymptotic forms, for a large time separation  $t$  and lattice time direction period  $T$ ,

$$C_{jr'r}^P(t) \rightarrow Z_{jr'r}^P \{ \exp(-m_j^P t) + \exp[-m_j^P (T - t)] \}, \quad (2.4)$$

$$C_{jr'r}^V(t) \rightarrow Z_{jr'r}^V \{ \exp(-m_j^V t) + \exp[-m_j^V (T - t)] \} \quad (2.5)$$

$$C_{jr'r}^A(t) \rightarrow Z_{jr'r}^A \{ \exp(-m_j^P t) + \exp[-m_j^P (T - t)] \}. \quad (2.6)$$

Here  $m_j^P$  and  $m_j^V$  are pseudoscalar and vector masses, respectively. Eqs. (2.4) and (2.6) imply, in addition, the asymptotic form

$$\frac{C_{jr'r''}^A(t)}{C_{jr'r}^P(t)} \rightarrow \frac{Z_{jr'r''}^A}{Z_{jr'r}^P}. \quad (2.7)$$

Measured in units of the lattice spacing  $a$  the decay constants  $f_j a$  and  $F_j a$  are then given, for any choice of smearing size  $r$ , by

$$(f_j a)^2 = \frac{2(z_j^A Z_{j0r}^{AP})^2}{m_j a Z_{jrr}^P} \quad (2.8)$$

$$(F_j a)^2 = \frac{2(z_j^V Z_{j0r}^{V})^2}{m_j a Z_{jrr}^V}. \quad (2.9)$$

The coefficients  $z_j^A$  and  $z_j^V$  are finite renormalizations chosen so that the lattice currents  $z_j^A a^3 J_{j0}^{5\mu}$  and  $z_j^V a^3 J_{j0}^\mu$  approach the continuum currents  $J_j^{5\mu}$  and  $J_j^\mu$ , respectively, as the lattice spacing approaches zero. These constants are often given the “naive” values

$$\begin{aligned} z_j^{AN} &= 2k_j^P, \\ z_j^{VN} &= 2k_j^V. \end{aligned} \quad (2.10)$$

where  $k_j^P$  and  $k_j^V$  are the hopping constants corresponding to the mass of the quark and antiquark for a pseudoscalar or vector meson, respectively, with flavor  $j$ , assumed here to have  $m_q = m_{\bar{q}}$ . A standard derivation of the naive finite renormalization constants, however, which relates the quark terms in the lattice action to those in the continuum action is actually not correct [8]. Although the naive finite renormalization constants do lead to the correct continuum limit, naive renormalization contributes to decay constant an additional extraneous dependence on lattice spacing. Numerical evidence for this behavior will be given in Section 7. A consistent calculation of finite renormalizations [8], correct to zeroth in a mean-field theory improved perturbation expansion, gives

$$\begin{aligned} z_j^{A0} &= 1 - \frac{3k_j^P}{4k_c}, \\ z_j^{V0} &= 1 - \frac{3k_j^V}{4k_c}, \end{aligned} \quad (2.11)$$

where  $k_c$  is the critical hopping constant at which the pion’s mass becomes zero. To first order in improved perturbation theory, the finite renormalizations become  $z_j^{A1} z^{A0}$

and  $z_j^{V1}z^{V0}$  where

$$\begin{aligned} z^{A1} &= 1 - 0.31\alpha_{\overline{m}s}(1/a), \\ z^{V1} &= 1 - 0.82\alpha_{\overline{m}s}(1/a). \end{aligned} \tag{2.12}$$

Decay constants for mesons with  $m_q \neq m_{\overline{q}}$  will be discussed below.

For equal values of the up and down quark masses,  $m_u$  and  $m_d$ , we adopt the convention that a missing flavor index  $j$  always has the value 1. Thus

$$\begin{aligned} C_{r'r}^P(t) &= C_{1r'r}^P(t), \\ Z_{r'r}^P &= Z_{1r'r}^P, \\ C_{r'r}^V(t) &= C_{1r'r}^V(t), \\ Z_{r'r}^V &= Z_{1r'r}^V, \\ C_{r'r}^A(t) &= C_{1r'r}^A(t), \\ Z_{r'r}^A &= Z_{1r'r}^A. \end{aligned} \tag{2.13}$$

### 3 PROPAGATORS

Table 1 lists the lattice sizes, parameter values, sweeps skipped between gauge configurations, and number of configurations used in the ensembles from which decay constants were calculated. Gauge configurations were generated with the Cabbibo-Marinari-Okawa algorithm. A variety of different test support the expectation that the large number of sweeps run between successive configurations were more than sufficient to produce statistically independent values for all of the quantities required by the present calculations. A discussion of the algorithms by which quark propagators were found is given in Ref. [1].

Vector and pseudoscalar masses and the coefficients  $Z_{r'r}^P$ ,  $Z_{r'r}^V$ , and  $Z_{r'r}^A$  were then determined by fitting  $C_{r'r}^P(t)$ ,  $C_{r'r}^V(t)$ , and  $C_{r'r}^A(t)$  to the asymptotic forms of Eqs. (2.4) - (2.6). As an alternative means of determining  $Z_{r'r}^A$  given a value of  $Z_{r'r}^P$ , fits of  $C_{r'r}^A(t)/C_{r'r}^P(t)$  were also made to the asymptotic form of Eqs. (2.7).

For the lattice  $8^3 \times 32$  at  $\beta$  of 5.70 we calculated propagators only for source  $r$  and sink  $r'$  of size 0. In all other cases we calculated propagators only for source size  $r$  of 2. To determine decay constants, according to Eqs. (2.8) and (2.9), fits for the lattice  $8^3 \times 32$  to propagators for the single sink of size 0 are sufficient, while for all other lattices fits are needed for sink sizes of both 0 and 2. To determine the range of time separations to be used in fitting for each  $\beta$  and  $k$  value, we evaluated effective masses  $m^P(t)$ ,  $m^V(t)$  and  $m^{P'}(t)$  by fitting  $C_{r'r}^P(t)$ ,  $C_{r'r}^V(t)$ , and  $C_{r'r}^A(t)$ , respectively, to Eqs. (2.4) - (2.6) at time separations  $t$  and  $t + 1$ . The largest interval at large  $t$  showing an approximate plateau in an effective mass graph we chose as the initial trial range on which to fit each propagator to the corresponding asymptotic form of Eqs. (2.4) - (2.6). Similarly, the largest interval at large  $t$  showing an approximate plateau in a graph of  $C_{r'r''}^A(t)/C_{r'r}^P(t)$  we chose as the initial trial range for a fit to Eq. (2.7). Figures (1) - (12) show the plateaus at large  $t$  in the effective masses  $m^P(t)$ ,  $m^{P'}(t)$ , the plateau at large  $t$  in the ratio  $C_{02}^A(t)/C_{02}^P(t)$ , and the effective mass  $m^V(t)$  for propagators with source  $r$  of 2 and sink  $r'$  of 0. Figures (1) - (4) show results for the lattice  $16^3 \times 32$  at  $\beta$  of 5.70 and the largest corresponding  $k$  value, 0.1675. Figures (5) - (8) show results for the lattice  $24^3 \times 36$  at  $\beta$  of 5.93 and the largest corresponding  $k$ , 0.1581. Figures (9) - (12) show results for  $30 \times 32^2 \times 40$  at  $\beta$  of 6.17 and the largest corresponding  $k$ , 0.1532.

Fits to data for a range of  $t$  were done by minimizing the fit's  $\chi^2$  determined from the full correlation matrix for the data being fit. An automatic fitting program repeatedly carried out fits on every connected interval of four or more points within the initial trial fitting range. For fits to Eq. (2.7), which require only a single fitting parameter, we looked at intervals of three or more points. The final fitting range was chosen by the program to be the interval with the smallest value of  $\chi^2$  per degree of freedom. Although a variety of other criteria could be used to determine the final fitting range, an advantage of the method we adopted is that it can be implemented automatically thereby reducing the potential for biases. The reliability of our in our final extrapolated results depends to some degree on adopting a consistent choice of fitting ranges at different parameter values.

The horizontal lines in Figures (1) - (12) show the fitted values of masses and

$Z_{02}^A/Z_{02}^P$ , and the pair of vertical lines in each figure indicates the interval of  $t$  values in the final fitting range chosen. It is perhaps useful to mention that since the effective mass at each  $t$  depends on data both at  $t$  and  $t + 1$ , the effective mass shown at the highest  $t$  within each final fitting range depends on data outside the fitting range. Thus the fitted lines tend to approximate the average of the effective masses within the fitting range but with the effective mass at highest  $t$  omitted. In all but one case, the data shows clear plateaus at large  $t$  extending over more than four time values. These plateaus appear to be fitted fairly reliably. For the rho propagator,  $C_{02}^V(t)$ , on the lattice  $24^3 \times 36$ , the plateau is more ambiguous. The fit is made over the four  $t$  values from 9 to 12, for which the three corresponding effective masses fall slowly. The effective masses at  $t$  of 12 to 15 then fall about one standard deviation below the fit. At  $t$  of 16 and 17, the effective masses then return to the original fitted value. This behavior is consistent with a statistical fluctuation although it makes the identification of the plateau at which to fit more ambiguous. Comparable ambiguities do not occur elsewhere in our data. The interval chosen is approximately a rescaling of the rho fitting intervals of 5 to 8, at  $\beta$  of 5.70 and 13 to 16, at  $\beta$  of 6.17. Also, the rho decay constant obtained from this fit in Section 4 interpolates smoothly values obtained from less ambiguous fits at other values of quark mass and lattice spacing. If this point were simply eliminated from our extrapolations of  $f_\rho$  in quark mass and in lattice spacing, our final continuum predictions would be nearly unchanged.

Value of  $\chi^2$  for the fits in Figures (1) - (12) are shown in Table 2. Our fits for sinks with size  $r'$  of 2, fits at smaller  $k$ , and fits on the lattice  $24^3 \times 32$  are of comparable quality to those shown and give comparable  $\chi^2$ .

Statistical uncertainties of parameters obtained from fits and of any function of these parameters were determined by the bootstrap method [7]. From each ensemble of  $N$  gauge configurations, 100 bootstrap ensembles were generated. Each bootstrap ensemble consists of a set of  $N$  gauge configurations randomly selected from the underlying  $N$  member ensemble allowing repeats. For each bootstrap ensemble the entire fit was repeated, including a possibly new choice of the final fitting interval. The collection of 100 bootstrap ensembles thus yields a collection of 100 values of any fitted parameter or any function of any fitted parameter. The statistical uncertainty

of any parameter is taken to be half the difference between a value which is higher than all but 15.9% of the bootstrap values and a value which is lower than all but 15.9% of the bootstrap values. In the limit of large  $N$  the collection of bootstrap values of a parameter  $p$  approaches a gaussian distribution and the definition we use for statistical uncertainty approaches the dispersion,  $d$ , given by  $\sqrt{\langle p^2 \rangle - \langle p \rangle^2}$ .

In the absence of some independent method for determining the predictions of QCD, it appears inevitable that the choice of  $t$  interval on which to fit data to a large  $t$  asymptotic form must be made by some procedure which depends on the Monte Carlo data itself. Thus the statistical uncertainties in the data lead to a corresponding uncertainty in the choice of fitting interval which, in turn, leads to some additional uncertainty in the fitted result. Another advantage of our procedure for choosing the fitting interval combined with bootstrap evaluation of statistical uncertainties is that the values we obtain for statistical uncertainties include the uncertainty arising from the choice of fitting interval. A comparison of the error bars found for our final fits with the error bars found using the same fitting range held fixed across the bootstrap ensemble shows that typically about 10% of the final statistical uncertainty comes from fluctuations over the bootstrap ensemble of the fitting range itself.

#### 4 DECAY CONSTANTS

To construct decay constants using the finite renormalizations of Eqs. (2.11) or (2.12), we require values of the critical hopping constant  $k_c$  and of the strong coupling constant  $\alpha_{\overline{m_s}}(1/a)$ . For  $k_c$  we used the values determined in Ref. [1]. These are listed in Table (3). To determine  $\alpha_{\overline{m_s}}(1/a)$  we first calculated  $\alpha_{\overline{m_s}}(\pi/a)$  using the mean-field improved perturbation theory relation [8, 4]

$$\frac{1}{g_{\overline{MS}}^2(\pi/a)} = \frac{\langle TrU/3 \rangle}{g_{lat}^2} + 0.025, \quad (4.1)$$

where  $\langle TrU \rangle$  is the expectation value of the trace of a plaquette and  $g_{lat}^2$  is  $6/\beta$ . We then found  $\alpha_{\overline{m_s}}(\pi/a)$  given by  $4\pi/g_{\overline{MS}}^2(\pi/a)$  and used the two-loop Callan-Symanzik equation to determine  $\alpha_{\overline{m_s}}(1/a)$ . The corresponding values of  $z^{A1}$  and  $z^{V1}$  are shown in Table (4).

Values of the decay constant in lattice units  $f_\pi a$  for the various lattices,  $\beta$  and  $k$  shown in Table (1) are listed in Tables (5) - (9). As a measure of the lattice spacing in each case, Table (10) gives the rho mass in lattice units  $m_\rho(m_n)a$ , extrapolated to the “normal” quark mass  $m_n$  which produces the physical value of  $m_\pi(m_n)/m_\rho(m_n)$  [1]. We list also values of  $m_n$  itself. These parameters are not given for the lattice  $8^3 \times 32$  since in this case we were not able to calculate propagators at small enough quark mass to perform the required extrapolation reliably. The finite renormalizations for the decay constants in Tables (5) - (9) all include both the leading term  $z^{A0}$  of Eqs. (2.11) and the first order mean-field improved perturbative correction  $z^{A1}$  of Eqs. (2.12). The second column in each table gives values of  $f_\pi a$  found from  $Z_{r'r}^A$  determined from a direct fit of  $C_{r'r}^A(t)$  to Eq. (2.6). The third column gives  $f_\pi a$  found from  $Z_{r'r}^A$  determined by fitting the ratio  $C_{r'r}^A(t)/C_{r'r}^P(t)$  to Eq. (2.7) and then using the value of  $Z_{r'r}^P$  found from a fit of  $C_{r'r}^P(t)$  to Eq. (2.4). The two sets of data in all cases are statistically consistent and in all cases, except for the lattice  $8^3 \times 32$  for  $k$  below 0.1500,  $f_\pi$  determined from ratio fits has a smaller statistical error  $f_\pi$  determined from direct fits. The ratio method tends to give less statistical noise, in effect, because it uses  $C_{r'r}^P(t)$ , which is relatively less noisy, to determine  $m^P$  and then extracts only  $Z_{r'r}^A$  from the more noisy propagator  $C_{r'r}^A(t)$ . The direct method extracts both  $Z_{r'r}^A$  and  $m^P$  from  $C_{r'r}^A(t)$  yielding an  $m^P$  with greater noise, which is then multiplied by a possibly large  $t$  and exponentiated, feeding additional noise back into the value of  $Z_{r'r}^A$ . In the remainder of this paper we use only values of  $f_\pi$  determined from ratio fits.

Values of the decay constant in lattice units  $F_\rho a$  for the lattices shown in Table (1) are listed in the fourth column of Tables (5) - (9). The finite renormalizations for  $F_\rho$  shown in these tables all include both the leading term  $z^{V0}$  of Eqs. (2.11) and the first order mean-field improved perturbative correction  $z^{V1}$  of Eqs. (2.12). The values of  $Z_{r'r}^V$  used to determine  $F_\rho$  were all extracted from direct fits of  $C_{r'r}^V(t)$  to Eq. (2.5).

## 5 VOLUME DEPENDENCE

Percentage changes in decay constants going from  $8^3 \times 32$  and  $16^3 \times 32$  to  $24^3 \times 32$ , at  $\beta$  of 5.70, are given in Table 11. These changes are the same for all choices of finite renormalization. All of the differences appear to be of marginal statistical significance and may therefore best be viewed as upper bounds on the volume dependence of our results. A variety of different arguments suggest that, for the range of  $k$ ,  $\beta$ , and lattice volume we have examined, the errors in valence approximation decay constants due to calculation in a finite volume  $L^3$  are bounded by an expression of the form  $Ce^{-L/R}$ . A simple non-relativistic potential model gives this expression with the radius of a hadron's wave function for  $R$ . A more elaborate field theory argument gives for  $R$  the Compton wave length of a pair of pions, which is the lightest state that can be exchanged between a pair of identical pseudoscalar or vector mesons. At  $\beta$  of 5.70,  $R$  is thus very likely to be between 3 and 5 lattice units. Since the changes in decay constants shown in Table 11 between  $16^3$  and  $24^3$  are all less than 5% for  $k \geq 0.1650$ , it follows that the differences between these values in  $24^3$  and in infinite volume should be less than 1.3%. For extrapolations to physical quark masses, we use only decay constants with  $k \geq 0.1650$ .

## 6 QUARK MASS EXTRAPOLATION

At the largest  $k$  on each lattice, the ratio  $m_\pi/m_\rho$  is significantly larger than its experimentally observed value of 0.179. Thus to produce decay constants for hadrons containing only light quarks, our data has to be extrapolated to larger  $k$  or, equivalently, to smaller quark mass. We did not calculate directly at larger  $k$  both because the algorithms we used to find quark propagators became too slow and because the statistical errors we found in trial calculations became too large.

Define the quark mass in lattice units  $m_q a$  to be

$$m_q a = \frac{1}{2k} - \frac{1}{2k_c}, \quad (6.1)$$

where  $k_c$  is the critical hopping constant at which  $m_\pi$  becomes zero. We found  $f_\pi a$

and  $F_\rho a$ , for all three possible choices of finite renormalization in Eqs. (2.10) - (2.12) to be nearly linear functions of  $m_q a$  over the entire range of  $k$  considered on each lattice.

Figure 13 shows  $f_\pi$  and  $F_\rho$ , with finite renormalizations including the first order mean-field improved perturbative correction, as functions of  $m_q$ . Data is shown from the three lattices of Table 1 which we use to evaluate continuum limits,  $16^3 \times 32$ ,  $24^3 \times 36$  and  $30 \times 32^2 \times 40$ . For convenience, decay constants at each  $\beta$  are shown in units of the central value of the rho mass  $m_\rho(m_n)$ , at the same  $\beta$ , extrapolated to the the “normal” quark mass  $m_n$ . Quark masses  $m_q$  for each  $\beta$  are shown in units of the central value of the strange quark mass  $m_s$  at the same  $\beta$ . The data Figure 13 has been scaled by the central values of  $m_\rho(m_n)$  and  $m_s$  taken as arbitrary external parameters, and the error bars shown do not include the effect of statistical fluctuations in  $m_\rho(m_n)$  or  $m_s$ . Table (10) gives values of  $m_s$  found in Ref. [1] by requiring  $m_\pi[(m_n + m_s)/2]/m_\rho(m_n)$  to be equal to the physical value of  $m_K/m_\rho$ . The lines in Figure 13 are fits of decay constants measured in lattice units,  $f_\pi a$  and  $F_\rho a$ , to linear functions of the quark mass in lattice units,  $m_q a$ , at the three smallest quark masses in the data set at each  $\beta$ . These fits were obtained by minimizing  $\chi^2$  obtained from the full correlation matrix among the data points. The correlation matrix was calculated by taking averages of data values and products of data values over bootstrap ensembles generated as described in Section (3). The  $\chi^2$  for these fits, and corresponding fits on the lattice  $24^3 \times 32$  at  $\beta$  of 5.70, are given in Table 12. The fits in Figure 13 appear to be quite good and provide, we believe, a reliable method for extrapolating decay constants down to light quark masses. With naive finite renormalization, Eq. (2.10), or zero order mean-field finite renormalization, Eq. (2.11),  $f_\pi a$  and  $F_\rho a$  fit straight lines in  $m_q a$  about as well as the first order perturbatively renormalized data of Figure 13.

The linear fits of Figure 13 permit the determination of  $f_K$  and  $F_\phi$  in addition to  $f_\pi$  and  $F_\rho$ . For a pion composed of a quark and antiquark with mass  $m_q \neq m_{\bar{q}}$ , Figure 13 suggests

$$f_\pi = \alpha_q m_q + \alpha_{\bar{q}} m_{\bar{q}} + \beta. \quad (6.2)$$

Charge conjugation invariance then gives  $\alpha_q = \alpha_{\bar{q}}$ . It follows that the kaon, which is a pion with, say,  $m_q = m_s$  and  $m_{\bar{q}} = m_n$ , will have the same decay constant as a pion composed of a single type of quark and antiquark with  $m_q = m_{\bar{q}} = (m_s + m_n)/2$ . On the other hand, the linear fits of Figure 13 permit  $F_\rho$  to be extrapolated to the point  $m_q = m_{\bar{q}} = m_s$  which, in the valence approximation, gives  $F_\phi$ . Tables 13 and 14 give the value of  $f_\pi a$ ,  $f_K a$ ,  $F_\rho a$  and  $F_\phi a$  obtained from the fits in Figure 13. The statistical uncertainties in these quantities were obtained by a further application of the bootstrap method of Section (3). Bootstrap ensembles of the underlying gauge configurations were generated, and on each bootstrap ensemble the extrapolated decay constants were recalculated. The uncertainty in each decay constant was obtained from the resulting distribution. The correlation matrices used to fit bootstrap data to linear functions of  $m_q a$  were taken to be the same as the correlation matrices for the full ensemble. To recalculate correlation matrices separately on each bootstrap ensemble by a further bootstrap would have been too time consuming.

## 7 CONTINUUM LIMIT

The ratios  $f_\pi/m_\rho$ ,  $f_K/m_\rho$ ,  $F_\rho/m_\rho$  and  $F_\phi/m_\rho$  for physical quark masses we then extrapolated to zero lattice spacing. For Wilson fermions the leading asymptotic lattice spacing dependence in these decay ratios is expected to be linear in  $a$ . On the other hand, as shown in Ref. [1],  $m_\rho a$  follows the two-loop Callan-Symanzik scaling prediction in  $\alpha_{\overline{MS}}$  quite well for the range of  $\beta$  considered here. Thus assuming the asymptotic form of the lattice spacing dependence of decay ratios appears to be reasonable. Figure 14 shows decay constants with first order perturbative renormalization along with fits to linear functions of  $m_\rho a$ . The quantity  $m_\rho a$  may be viewed as the lattice spacing  $a$  measured in units of the physical rho Compton wavelength,  $1/m_\rho$ . The vertical bars at  $m_\rho a$  of 0, offset slightly for visibility, are the extrapolated predictions' uncertainties. The horizontal lines at  $m_\rho a$  of 0 lying within or slightly above the range of each prediction are the corresponding experimental values. The data points in Figure 14 are from the lattices  $16^3 \times 32$ ,  $24^3 \times 36$  and  $30 \times 32^2 \times 40$ . The values of  $\beta$  for these lattices were chosen so that the physical volume in each

case is nearly the same. For lattice period  $L$ , the quantity  $m_\rho L$  is respectively,  $9.08 \pm 0.13$ ,  $9.24 \pm 0.19$  and, averaged over three directions,  $8.67 \pm 0.12$  [1].

The fits shown in Figure 14 were found by minimizing  $\chi^2$  obtained from the full correlation matrix among the fitted data. Since both the x and y coordinates of each of the three fitted points on each line have statistical uncertainties, we evaluated  $\chi^2$  among all six pieces of data and chose as fitting parameters the slope and intercept of the line along with the x coordinate of each point. The required correlation matrices were found by the bootstrap method as were the statistical uncertainties of the extrapolated predictions. The correlation matrices used in fits for each bootstrap ensemble were again taken from the full ensemble and not recalculated on each bootstrap ensemble independently. The  $\chi^2$  per degree of freedom for the fits in Figure 14, are given in Table 15.

For the lattice spacing dependence of decay ratios found using zeroth order mean-field finite renormalization and using naive finite renormalization we also made fits to linear functions of  $m_\rho a$ . The slopes with respect to  $m_\rho a$  of the ratios  $f_\pi/m_\rho$ ,  $f_K/m_\rho$ ,  $F_\rho/m_\rho$  and  $F_\phi/m_\rho$  along with  $\chi^2$  for each fit are also given in Table 15. It is clear from these results, as mentioned in Section 2, that naive renormalization leads to decay ratios with significantly stronger lattice spacing dependence than found for either zeroth or first order improved perturbative renormalization. There also appears to be some tendency for first order perturbative renormalization to lead to weaker lattice spacing dependence than zeroth order. It follows that the extrapolations we have done to zero lattice spacing are likely to be most reliable for first order perturbative renormalization and least reliable for naive renormalization.

## 8 INFINITE VOLUME LIMIT

The continuum ratios we found in finite volume were then corrected to infinite volume by an adaptation of the method used in Ref. [1] to correct finite volume continuum mass ratios to infinite volume. From  $f_\pi/m_\rho$ , with first order perturbative renormalization, as a function of lattice spacing  $a$  and lattice period  $L$ , both measured

in physical units, define the finite volume correction term  $\Delta(a, L)$  to be

$$\Delta(a, L) = \frac{f_\pi}{m_\rho}(a, \infty) - \frac{f_\pi}{m_\rho}(a, L). \quad (8.1)$$

The quantity which we would like to determine is  $\Delta(0, 9/m_\rho)$ . Now the ratio  $f_\pi/m_\rho$ , for  $L$  of  $9/m_\rho$ , undergoes a relative change of a bit less than 20% as  $a$  goes from its value  $a_{5.7}$  at  $\beta$  of 5.70 to 0. Thus we would expect an error of about 20% of  $\Delta(0, 9/m_\rho)$  for the approximation

$$\Delta(0, \frac{9}{m_\rho}) \approx \Delta(a_{5.7}, \frac{9}{m_\rho}). \quad (8.2)$$

Moreover, from our earlier discussion of the exponential approach of decay ratios to their infinite volume limits, it follows that with an additional error of about 20% of  $\Delta(0, 9/m_\rho)$  we have

$$\Delta(a_{5.7}, \frac{9}{m_\rho}) \approx \frac{f_\pi}{m_\rho}(a_{5.7}, \frac{13.5}{m_\rho}) - \frac{f_\pi}{m_\rho}(a_{5.7}, \frac{9}{m_\rho}), \quad (8.3)$$

where  $L$  of  $13.5/m_\rho$  corresponds to the lattice  $24^3 \times 32$  at  $\beta$  of 5.70. Finally, a direct evaluation of the right side of Eq. (8.3) shows it is quite small, with statistical errors of about 6% of  $f_\pi/m_\rho$ . Combining Eqs. (8.1) - (8.3), we obtain

$$\frac{f_\pi}{m_\rho}(0, \infty) \approx \frac{f_\pi}{m_\rho}(0, \frac{9}{m_\rho}) + \frac{f_\pi}{m_\rho}(a_{5.7}, \frac{13.5}{m_\rho}) - \frac{f_\pi}{m_\rho}(a_{5.7}, \frac{9}{m_\rho}). \quad (8.4)$$

The error in this approximation should be less than about 40% of 6% of  $f_\pi/m_\rho$ , which is 2.4% of  $f_\pi/m_\rho$ . Table 16 lists estimates of the systematic uncertainties in equations corresponding to Eq. (8.4) for other decay constants and other choices of finite renormalization. First order perturbative renormalization consistently gives the smallest systematic error in volume correction largely because the lattice spacing dependence of these decay ratios is smallest.

The ratios  $f_\pi/m_\rho$ ,  $f_K/m_\rho$ ,  $F_\rho/m_\rho$  and  $F_\phi/m_\rho$ , for all three different choices of finite renormalization, extrapolated to zero lattice spacing with  $m_\rho L$  fixed at 9, and then corrected to infinite volume are shown in Table 17. For first order perturbative

renormalization we also give, in Table 18, finite and infinite volume values of the ratios  $f_\pi/f_K$ ,  $F_\rho/f_K$  and  $F_\phi/f_K$ . The errors shown for infinite volume ratios are statistical only and do not include the estimates we have just given for the systematic error in our procedure for making infinite volume corrections. For first order perturbative finite renormalization, a comparison of Tables 16 and 17 shows, however, that the systematic errors arising from our method of obtaining infinite volume results are much smaller than the statistical errors. For the range of  $\beta$  used in our extrapolation to zero lattice spacing, first order mean-field theory improved perturbation expansions have been shown [8] to work quite well for a wide variety of different quantities. In addition, as we mentioned earlier, the extrapolation to zero lattice spacing should be most reliable for this renormalization scheme. Thus we believe that the numbers in Table 17 obtained using first order mean-field perturbative renormalization are significantly more reliable than those found using the other two renormalization methods. Zeroth order perturbative renormalization has been included, however, to provide some measure of the degree to which our results may be sensitive to the choice of renormalization. Half of the difference between first order and zeroth order mean-field perturbative renormalization appears to us to be a conservative estimate of the systematic uncertainty in the first order results arising from the missing second and higher order perturbative renormalization contributions. In all cases this uncertainty is significantly less than the statistical errors. Predictions obtained with naive renormalization have been included in Table 17 largely as a curiosity. It is interesting to notice, however, that the difference between the final, infinite volume results found with naive renormalization and those found with first order perturbative renormalization is still less than 1.5 times the naive renormalization statistical errors.

The predicted infinite volume ratios in Table 17 are all statistically consistent with the corresponding finite volume ratios. The main consequence of the correction to infinite volume is an increase in the size of the statistical uncertainty in each prediction.

The experimental numbers shown in Table 17 for  $f_\pi$  and  $f_K$  are from charged particle decays and for  $f_\rho$  from neutral decays. In all cases the uncertainties in the experimental values are 0.001 or less. As mentioned in the introduction, an

experimental value for the neutral pion decay [3] gives  $f_\pi/m_\rho$  of  $0.110 \pm 0.005$ , which is quite close to our prediction. The systematic uncertainties in this experimental number, however, are larger than those for the charged pion decay. As a result the significance of the improved agreement of our prediction with the observed neutral pion decay constant is unclear to us.

We would like to thank Paul Mackenzie for discussions, and Mike Cassera, Molly Elliott, Dave George, Chi Chai Huang and Ed Nowicki for their work on GF11. We are particularly grateful to Chris Sachrajda for calling our attention to an error in an earlier version of this paper.

## References

- [1] F. Butler, H. Chen, J. Sexton, A. Vaccarino and D. Weingarten, *Physical Review Letters* 70, 2849 (1993).
- [2] D. Toussaint, *Nucl. Phys. B (Proc. Suppl.)* 26 (1992) 3.
- [3] H.-J. Behrend et al., *Z. Phys. C* 49 (1991) 401.
- [4] A. X. El-Khadra, G. H. Hockney, A. S. Kronfeld and P. B. Mackenzie, *Phys. Rev. Letts.* 69 (1992) 729.
- [5] D. H. Weingarten, *Phys. Lett.* 109B, 57 (1982); *Nuclear Physics*, B215 [FS7], 1 (1983).
- [6] D. Weingarten, *Nucl. Phys. B (Proc. Suppl.)* 17 (1990) 272.
- [7] B. Efron, *The Jackknife, the Bootstrap and Other Resampling Plans*, Society for Industrial and Applied Mathematics, Philadelphia, 1982.
- [8] G. P. Lepage and P. B. Mackenzie, to appear in *Physical Review D* 48 (1993).

lattice	$\beta$	k	skip	count
$8^3 \times 32$	5.70	0.1400 - 0.1650	1000	2439
$16^3 \times 32$	5.70	0.1600 - 0.1675	2000	219
$24^3 \times 32$	5.70	0.1600 - 0.1675	4000	58
$24^3 \times 36$	5.93	0.1543 - 0.1581	4000	210
$30 \times 32^2 \times 40$	6.17	0.1500 - 0.1532	6000	219

Table 1: Configurations analyzed.

lattice	$\beta$	$C_{02}^P$	$C_{02}^A$	$C_{02}^A/C_{02}^P$	$C_{02}^V$
$16^3 \times 32$	5.70	0.09	0.22	0.23	0.11
$24^3 \times 36$	5.93	0.08	0.07	0.47	0.68
$30 \times 32^2 \times 40$	6.17	0.16	0.10	0.01	0.25

Table 2: Values of  $\chi^2$  per degree of freedom for fits to propagators.

lattice	$\beta$	$k_c$
$8^3 \times 32$	5.70	$0.169012 \pm 0.000102$
$16^3 \times 32$	5.70	$0.169405 \pm 0.000052$
$24^3 \times 32$	5.70	$0.169304 \pm 0.000035$
$24^3 \times 36$	5.93	$0.158948 \pm 0.000026$
$30 \times 32^2 \times 40$	6.17	$0.153763 \pm 0.000018$

Table 3: Critical hopping constant values.

$\beta$	$z^{A1}$	$z^{V1}$
5.70	0.93269	0.82194
5.93	0.94208	0.84679
6.17	0.94828	0.86320

Table 4: First order perturbative correction factors to finite renormalizations.

k	$f_\pi a$ direct	$f_\pi a$ ratio	$F_\rho a$
0.1400	$0.2346 \pm 0.0011$	$0.2347 \pm 0.0011$	$0.2861 \pm 0.0015$
0.1450	$0.2080 \pm 0.0014$	$0.2083 \pm 0.0010$	$0.2684 \pm 0.0014$
0.1500	$0.1811 \pm 0.0016$	$0.1820 \pm 0.0010$	$0.2505 \pm 0.0017$
0.1550	$0.1532 \pm 0.0018$	$0.1538 \pm 0.0012$	$0.2316 \pm 0.0026$
0.1600	$0.1238 \pm 0.0022$	$0.1243 \pm 0.0012$	$0.2074 \pm 0.0022$
0.1650	$0.0895 \pm 0.0074$	$0.0925 \pm 0.0021$	$0.1843 \pm 0.0043$

Table 5: Decay constants in lattice units measured on a lattice  $8^3 \times 32$  at  $\beta = 5.70$ . Finite renormalizations include the first order perturbative correction.

k	$f_\pi a$ direct	$f_\pi a$ ratio	$F_\rho a$
0.1600	$0.1212 \pm 0.0040$	$0.1236 \pm 0.0016$	$0.1975 \pm 0.0047$
0.1650	$0.0915 \pm 0.0046$	$0.0947 \pm 0.0019$	$0.1840 \pm 0.0069$
0.16625	$0.0799 \pm 0.0061$	$0.0875 \pm 0.0022$	$0.1794 \pm 0.0061$
0.1675	$0.0720 \pm 0.0098$	$0.0818 \pm 0.0025$	$0.1794 \pm 0.0034$

Table 6: Decay constants in lattice units measured on a lattice  $16^3 \times 32$  at  $\beta = 5.70$ . Finite renormalizations include the first order perturbative correction.

k	$f_\pi a$ direct	$f_\pi a$ ratio	$F_\rho a$
0.1600	$0.1251 \pm 0.0026$	$0.1249 \pm 0.0010$	$0.2116 \pm 0.0035$
0.1650	$0.0951 \pm 0.0031$	$0.0940 \pm 0.0010$	$0.1930 \pm 0.0055$
0.1663	$0.0792 \pm 0.0083$	$0.0860 \pm 0.0015$	$0.1865 \pm 0.0052$
0.1675	$0.0769 \pm 0.0059$	$0.0787 \pm 0.0018$	$0.1752 \pm 0.0043$

Table 7: Decay constants in lattice units measured on a lattice  $24^3 \times 32$  at  $\beta = 5.70$ . Finite renormalizations include the first order perturbative correction.

k	$f_\pi a$ direct	$f_\pi a$ ratio	$F_\rho a$
0.1543	$0.0763 \pm 0.0025$	$0.0729 \pm 0.0009$	$0.1187 \pm 0.0030$
0.1560	$0.0668 \pm 0.0037$	$0.0625 \pm 0.0008$	$0.1096 \pm 0.0043$
0.1573	$0.0562 \pm 0.0021$	$0.0544 \pm 0.0009$	$0.1077 \pm 0.0033$
0.1581	$0.0517 \pm 0.0029$	$0.0490 \pm 0.0012$	$0.1027 \pm 0.0037$

Table 8: Decay constants in lattice units measured on a lattice  $24^3 \times 36$  at  $\beta = 5.93$ . Finite renormalizations include the first order perturbative correction.

k	$f_\pi a$ direct	$f_\pi a$ ratio	$F_\rho a$
0.1500	$0.0557 \pm 0.0009$	$0.0566 \pm 0.0005$	$0.0852 \pm 0.0008$
0.1519	$0.0444 \pm 0.0012$	$0.0449 \pm 0.0004$	$0.0760 \pm 0.0010$
0.1526	$0.0403 \pm 0.0017$	$0.0400 \pm 0.0005$	$0.0724 \pm 0.0013$
0.1532	$0.0361 \pm 0.0023$	$0.0356 \pm 0.0007$	$0.0696 \pm 0.0028$

Table 9: Decay constants in lattice units measured on a lattice  $30 \times 32^2 \times 40$  at  $\beta = 6.17$ . Finite renormalizations include the first order perturbative correction.

lattice	$\beta$	$m_\rho a$	$m_n a$	$m_s a$
$16^3 \times 32$	5.70	$0.5676 \pm 0.0079$	$0.00390 \pm 0.00012$	$0.09662 \pm 0.00291$
$24^3 \times 32$	5.70	$0.5409 \pm 0.0089$	$0.00348 \pm 0.00012$	$0.08620 \pm 0.00303$
$24^3 \times 36$	5.93	$0.3851 \pm 0.0079$	$0.00223 \pm 0.00009$	$0.05536 \pm 0.00226$
$30 \times 32^2 \times 40$	6.17	$0.2768 \pm 0.0039$	$0.00141 \pm 0.00004$	$0.03503 \pm 0.00096$

Table 10: The normal and strange quark masses,  $m_n$  and  $m_s$ , and the rho mass extrapolated to quark mass  $m_n$ .

decay	k	$f(24^3) - f(8^3)$	$f(24^3) - f(16^3)$
$f_\pi$	0.1600	$0.4 \pm 1.4\%$	$1.0 \pm 1.5\%$
	0.1650	$1.7 \pm 2.6\%$	$-0.7 \pm 2.3\%$
	0.1663		$-1.7 \pm 3.3\%$
	0.1675		$-4.1 \pm 4.1\%$
$F_\rho$	0.1600	$2.0 \pm 1.7\%$	$6.7 \pm 2.9\%$
	0.1650	$4.5 \pm 3.9\%$	$4.7 \pm 5.1\%$
	0.1663		$3.8 \pm 4.6\%$
	0.1675		$-2.4 \pm 2.8\%$

Table 11: Changes in decay constants from  $8^3 \times 32$  to  $24^3 \times 32$  and from  $16^3 \times 32$  to  $24^3 \times 32$  at  $\beta = 5.70$

lattice	$\beta$	$\chi^2$ for $f_\pi$	$\chi^2$ for $F_\rho$
$16^3 \times 32$	5.70	0.256	0.149
$24^3 \times 32$	5.70	0.003	0.180
$24^3 \times 36$	5.93	0.394	0.358
$30 \times 32^2 \times 40$	6.17	0.130	0.014

Table 12: Values of  $\chi^2$  for fits of decay constants to linear functions of  $m_q$  at the three smallest values of  $m_q$ .

lattice	$\beta$	$f_\pi a$	$f_K a$
$16^3 \times 32$	5.70	$0.0724 \pm 0.0030$	$0.0861 \pm 0.0017$
$24^3 \times 32$	5.70	$0.0691 \pm 0.0025$	$0.0831 \pm 0.0016$
$24^3 \times 36$	5.93	$0.0449 \pm 0.0012$	$0.0532 \pm 0.0008$
$30 \times 32^2 \times 40$	6.17	$0.0323 \pm 0.0008$	$0.0378 \pm 0.0005$

Table 13: Decay constants in lattice units extrapolated to physical quark mass.

lattice	$\beta$	$F_\rho a$	$F_\phi a$
$16^3 \times 32$	5.70	$0.1747 \pm 0.0076$	$0.1870 \pm 0.0107$
$24^3 \times 32$	5.70	$0.1642 \pm 0.0070$	$0.1975 \pm 0.0063$
$24^3 \times 36$	5.93	$0.1014 \pm 0.0047$	$0.1098 \pm 0.0037$
$30 \times 32^2 \times 40$	6.17	$0.0668 \pm 0.0026$	$0.0748 \pm 0.0012$

Table 14: Decay constants in lattice units extrapolated to physical quark mass.

decay	renorm.	slope	$\chi^2$
$f_\pi/m_\rho$	first order perturb.	$0.035 \pm 0.022$	0.62
	zeroth order perturb.	$0.044 \pm 0.023$	0.61
	naive	$0.112 \pm 0.030$	0.74
$f_K/m_\rho$	first order perturb.	$0.052 \pm 0.016$	1.04
	zeroth order perturb.	$0.063 \pm 0.017$	1.02
	naive	$0.112 \pm 0.022$	0.99
$F_\rho/m_\rho$	first order perturb.	$0.228 \pm 0.047$	0.04
	zeroth order perturb.	$0.325 \pm 0.058$	0.06
	naive	$0.546 \pm 0.075$	0.19
$F_\phi/m_\rho$	first order perturb.	$0.192 \pm 0.061$	0.20
	zeroth order perturb.	$0.286 \pm 0.073$	0.22
	naive	$0.362 \pm 0.091$	0.20

Table 15: Slope and  $\chi^2$  of fits of decay ratios' lattice spacing dependence to linear functions of  $m_\rho a$ .

decay	renorm.	error
$f_\pi/m_\rho$	first order perturb.	2%
	zeroth order perturb.	3%
	naive	4%
$f_K/m_\rho$	first order perturb.	2%
	zeroth order perturb.	2%
	naive	2%
$F_\rho/m_\rho$	first order perturb.	6%
	zeroth order perturb.	7%
	naive	10%
$F_\phi/m_\rho$	first order perturb.	8%
	zeroth order perturb.	10%
	naive	12%

Table 16: Estimated systematic errors in infinite volume quantities arising from the correction from finite volume to infinite volume.

decay	renorm.	finite volume	infinite volume	obs.
$f_\pi/m_\rho$	first order perturb.	$0.106 \pm 0.009$	$0.106 \pm 0.014$	0.121
	zeroth order perturb.	$0.110 \pm 0.009$	$0.110 \pm 0.015$	
	naive	$0.119 \pm 0.011$	$0.120 \pm 0.019$	
$f_K/m_\rho$	first order perturb.	$0.121 \pm 0.006$	$0.123 \pm 0.009$	0.148
	zeroth order perturb.	$0.125 \pm 0.007$	$0.127 \pm 0.010$	
	naive	$0.141 \pm 0.008$	$0.144 \pm 0.013$	
$F_\rho/m_\rho$	first order perturb.	$0.177 \pm 0.021$	$0.173 \pm 0.029$	0.199
	zeroth order perturb.	$0.189 \pm 0.024$	$0.184 \pm 0.036$	
	naive	$0.191 \pm 0.030$	$0.186 \pm 0.045$	
$F_\phi/m_\rho$	first order perturb.	$0.217 \pm 0.019$	$0.253 \pm 0.035$	0.219
	zeroth order perturb.	$0.234 \pm 0.023$	$0.277 \pm 0.043$	
	naive	$0.269 \pm 0.029$	$0.328 \pm 0.052$	

Table 17: Calculated values of meson decay constants extrapolated to zero lattice spacing in finite volume, then corrected to infinite volume, compared with observed values.

decay	finite volume	infinite volume	obs.
$f_\pi/f_K$	$0.875 \pm 0.034$	$0.864 \pm 0.065$	0.818
$F_\rho/f_K$	$1.467 \pm 0.170$	$1.412 \pm 0.229$	1.345
$F_\phi/f_K$	$1.795 \pm 0.131$	$2.058 \pm 0.283$	1.480

Table 18: Calculated values of meson decay constants, using first order perturbative renormalization, extrapolated to zero lattice spacing in finite volume, then corrected to infinite volume, compared with observed values.

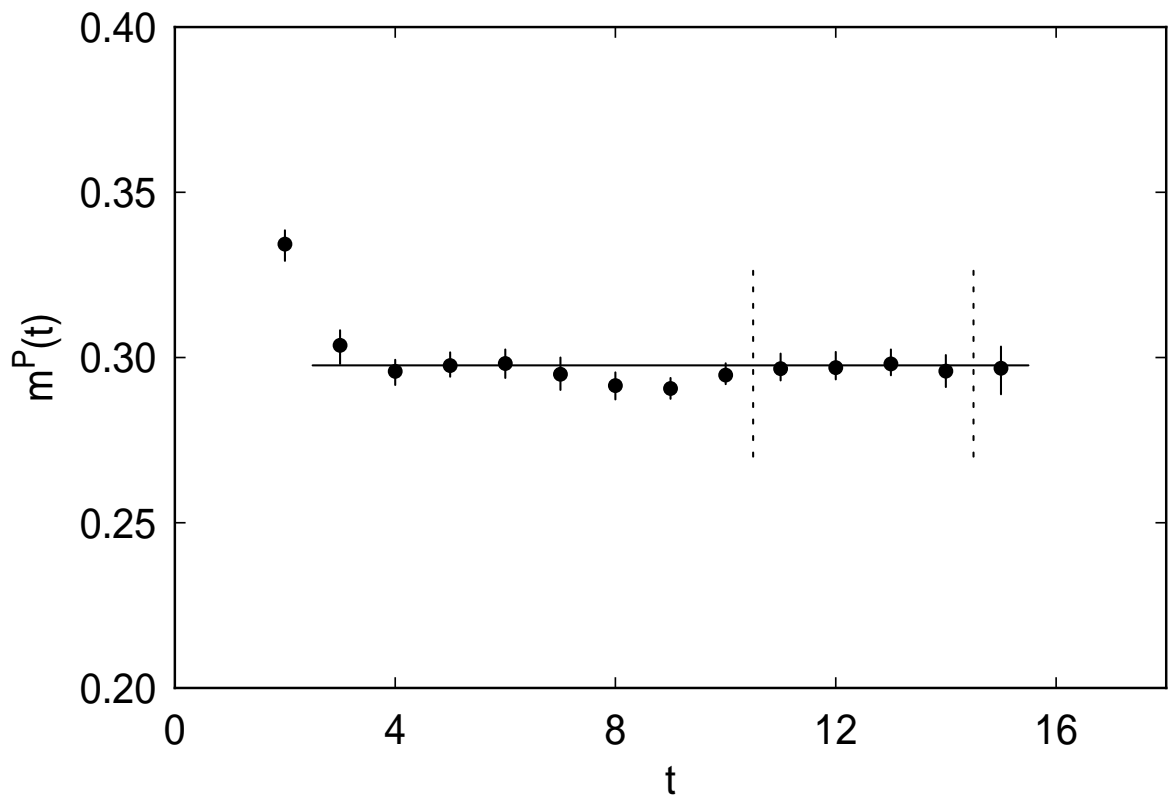


Figure 1: Effective masses and fitted mass for the pseudoscalar propagator  $C_{02}^P(t)$  on the lattice  $16^3 \times 32$  at  $\beta = 5.70$  and  $k = 0.1675$

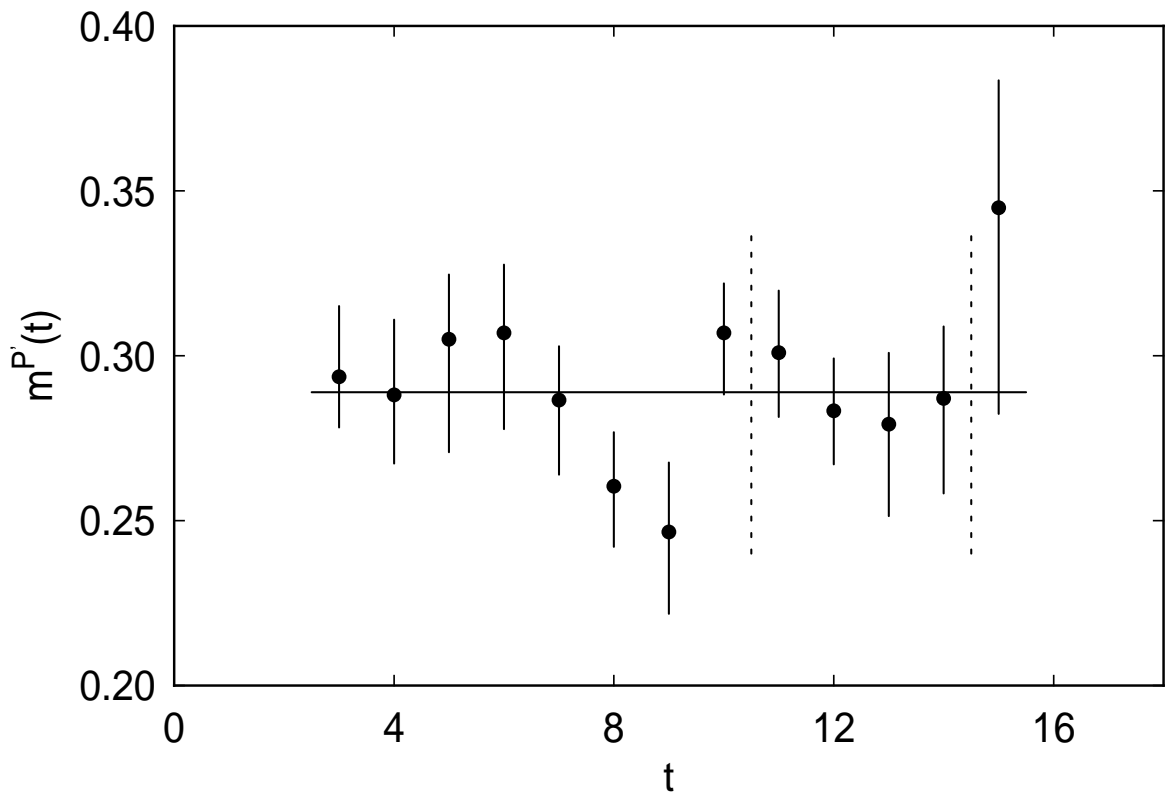


Figure 2: Effective masses and fitted mass for the axial vector propagator  $C_{02}^A(t)$  on the lattice  $16^3 \times 32$  at  $\beta = 5.70$  and  $k = 0.1675$

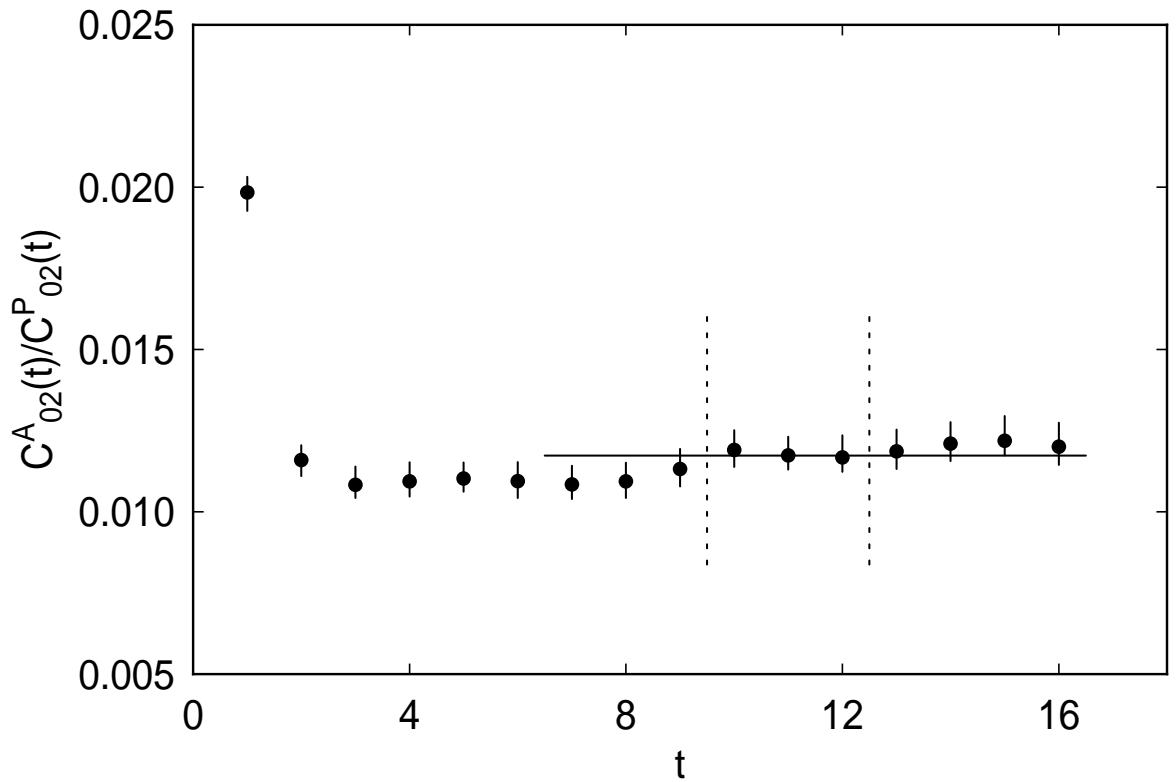


Figure 3: The propagator ratio  $C_{02}^A(t)/C_{02}^P(t)$  and a fit to its large  $t$  plateau on the lattice  $16^3 \times 32$  at  $\beta = 5.70$  and  $k = 0.1675$

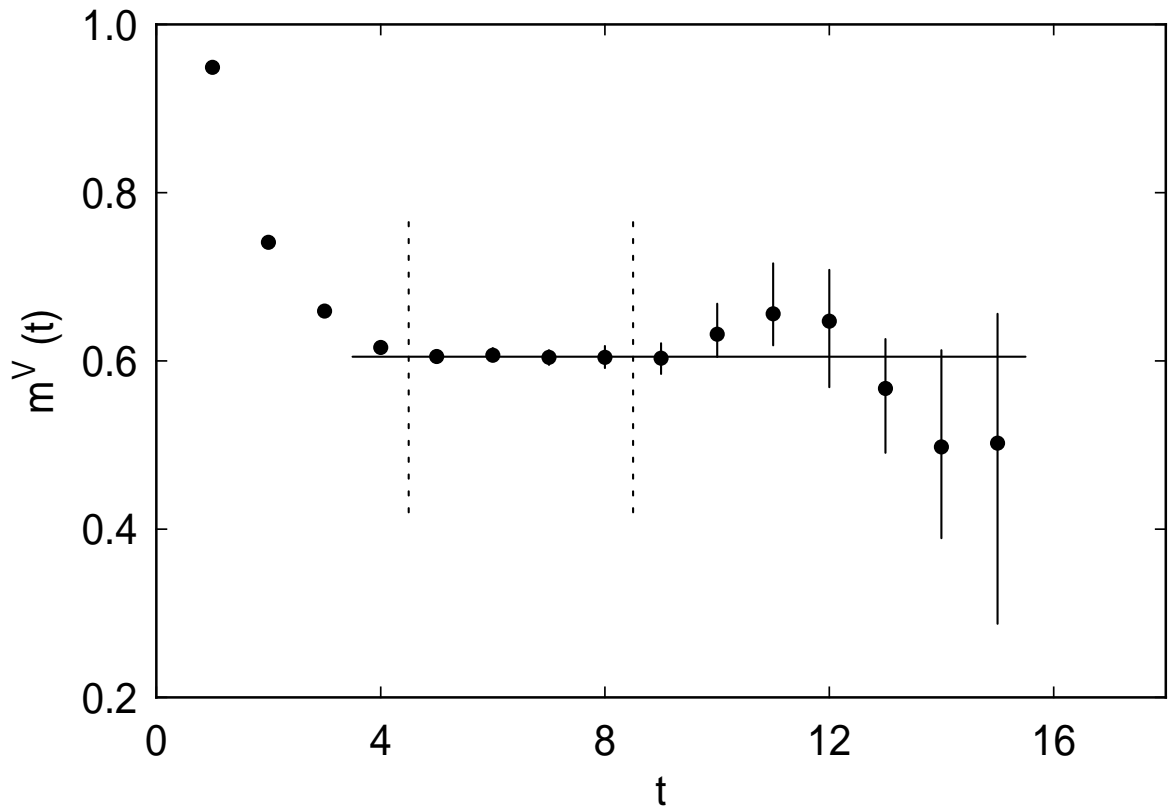


Figure 4: Effective masses and fitted mass for the vector propagator  $C_{02}^V(t)$  on the lattice  $16^3 \times 32$  at  $\beta = 5.70$  and  $k = 0.1675$

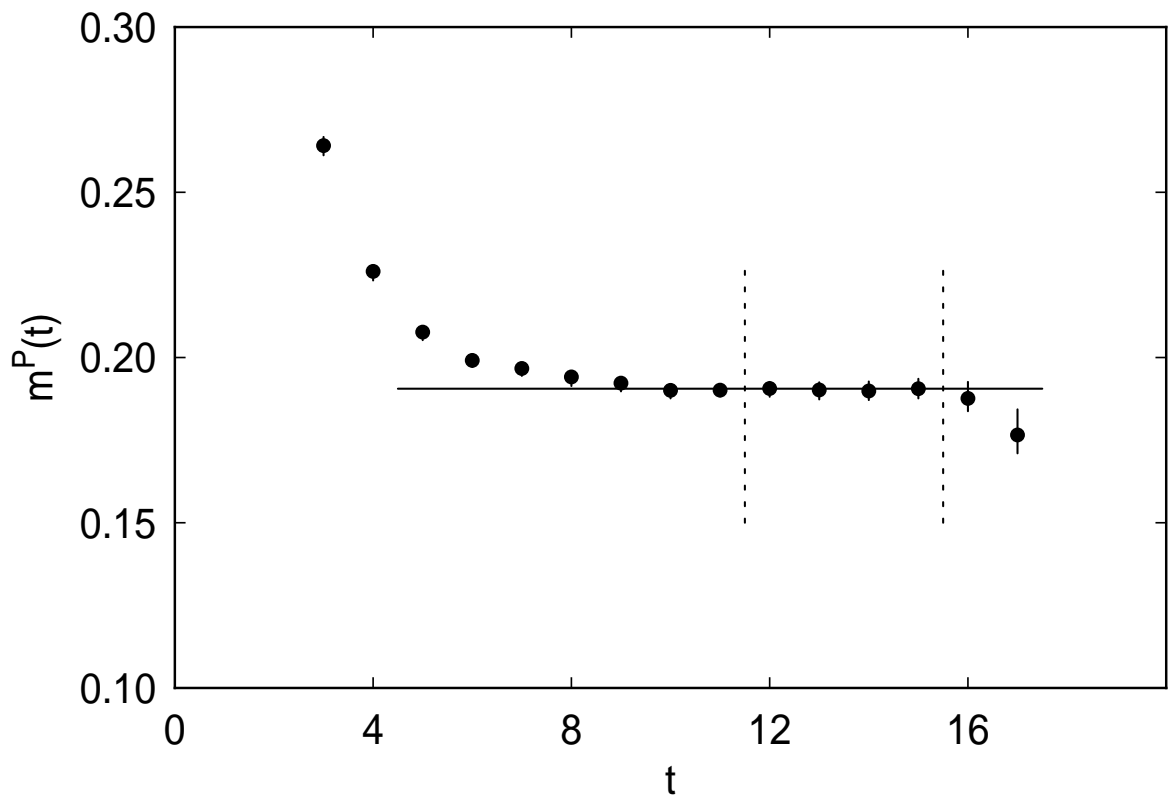


Figure 5: Effective masses and fitted mass for the pseudoscalar propagator  $C_{02}^P(t)$  on the lattice  $24^3 \times 36$  at  $\beta = 5.93$  and  $k = 0.1581$

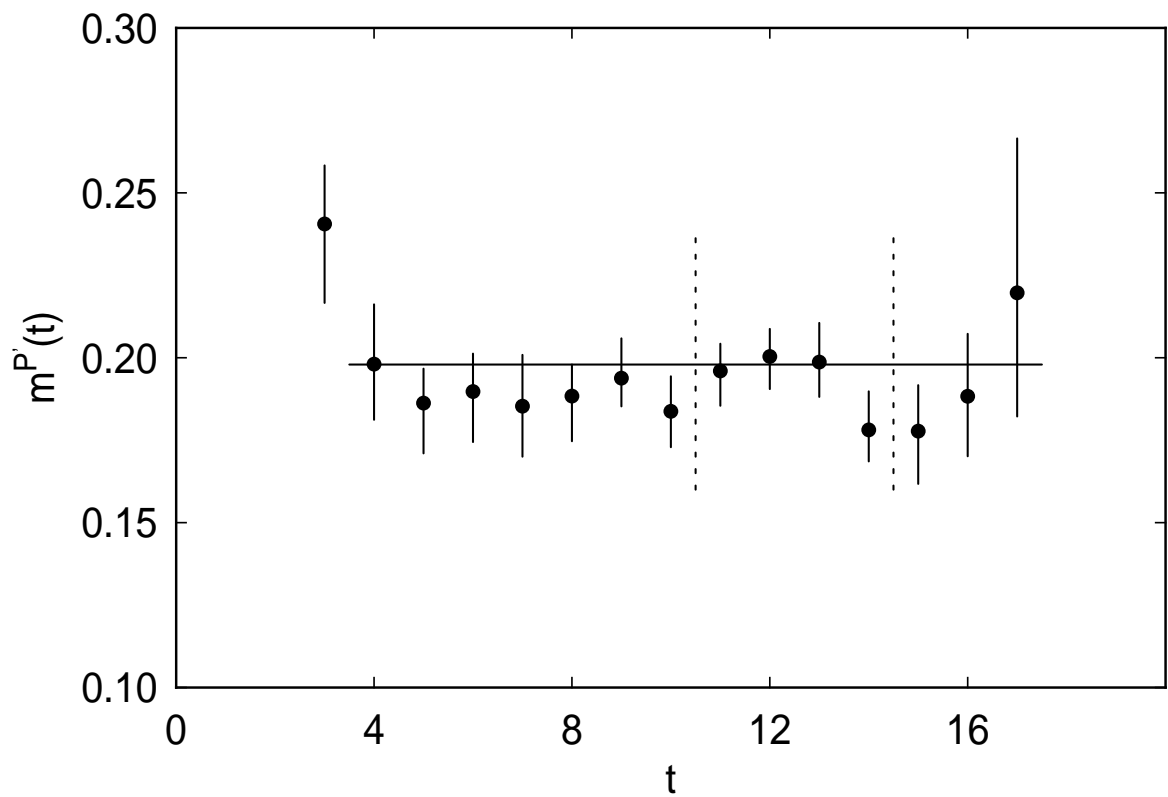


Figure 6: Effective masses and fitted mass for the axial vector propagator  $C_{02}^A(t)$  on the lattice  $24^3 \times 36$  at  $\beta = 5.93$  and  $k = 0.1581$

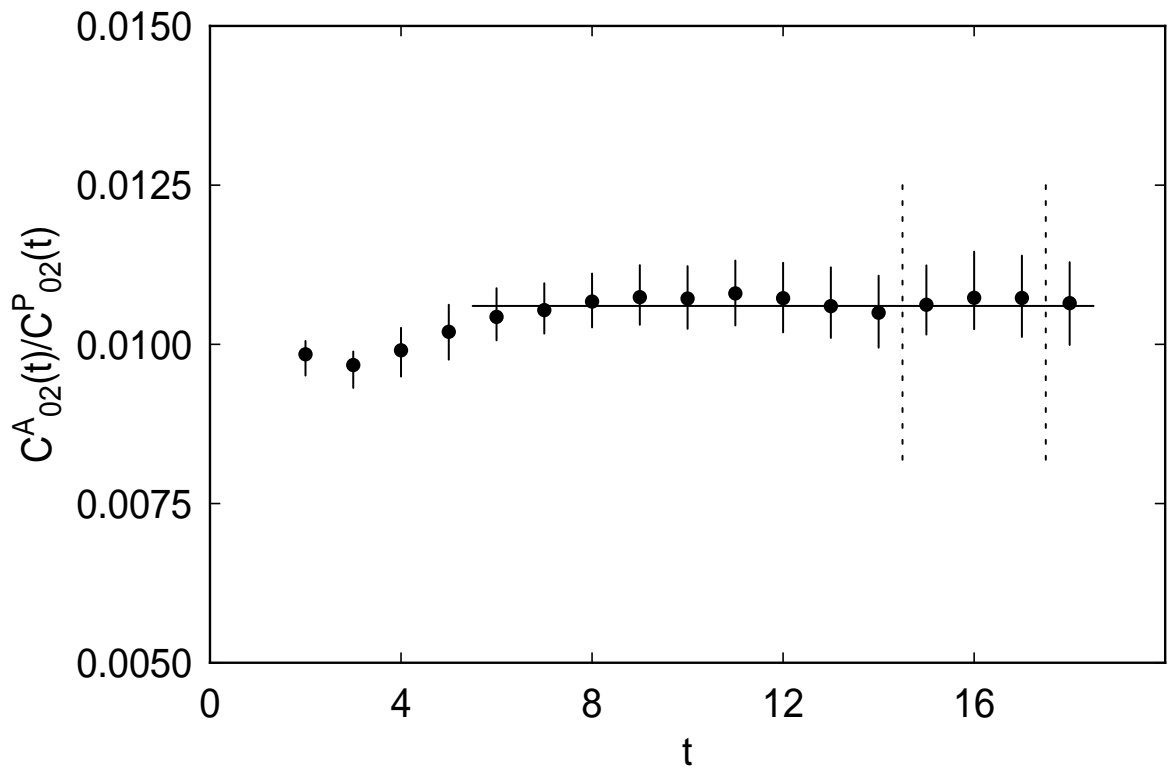


Figure 7: The propagator ratio  $C_{02}^A(t)/C_{02}^P(t)$  and a fit to its large  $t$  plateau on the lattice  $24^3 \times 36$  at  $\beta = 5.93$  and  $k = 0.1581$

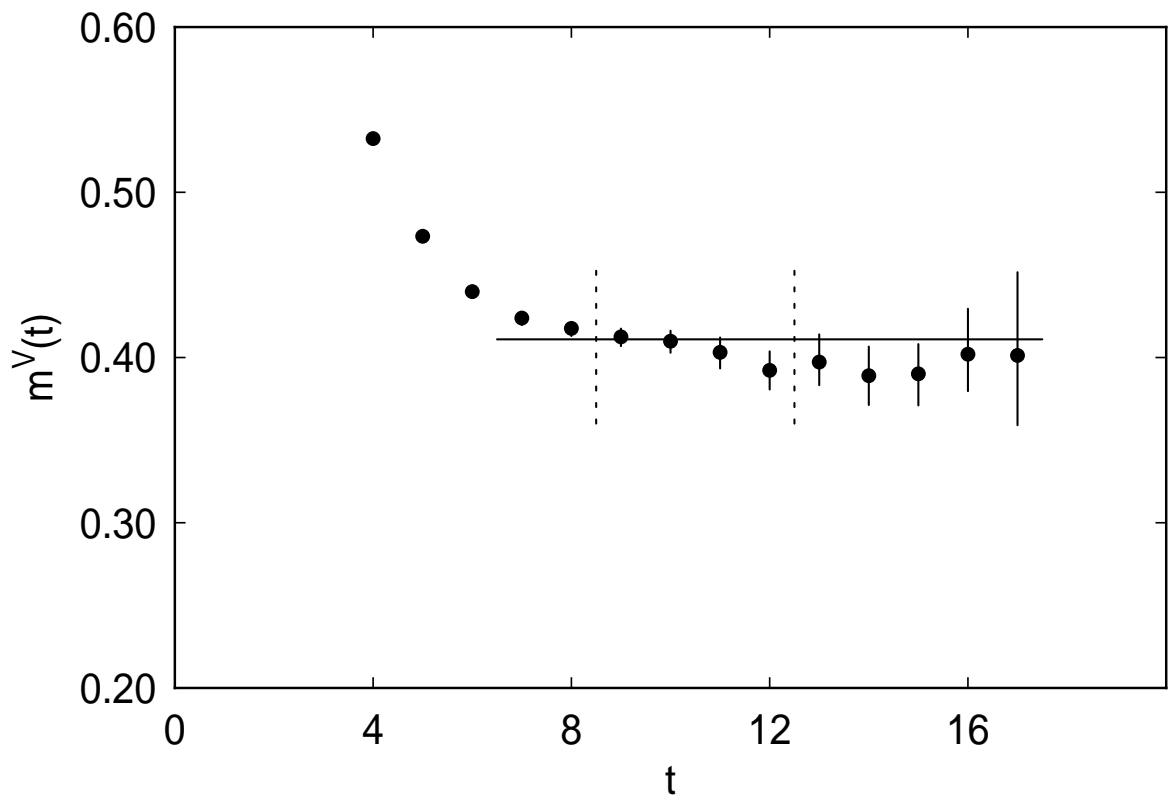


Figure 8: Effective masses and fitted mass for the vector propagator  $C_{02}^V(t)$  on the lattice  $24^3 \times 36$  at  $\beta = 5.93$  and  $k = 0.1581$

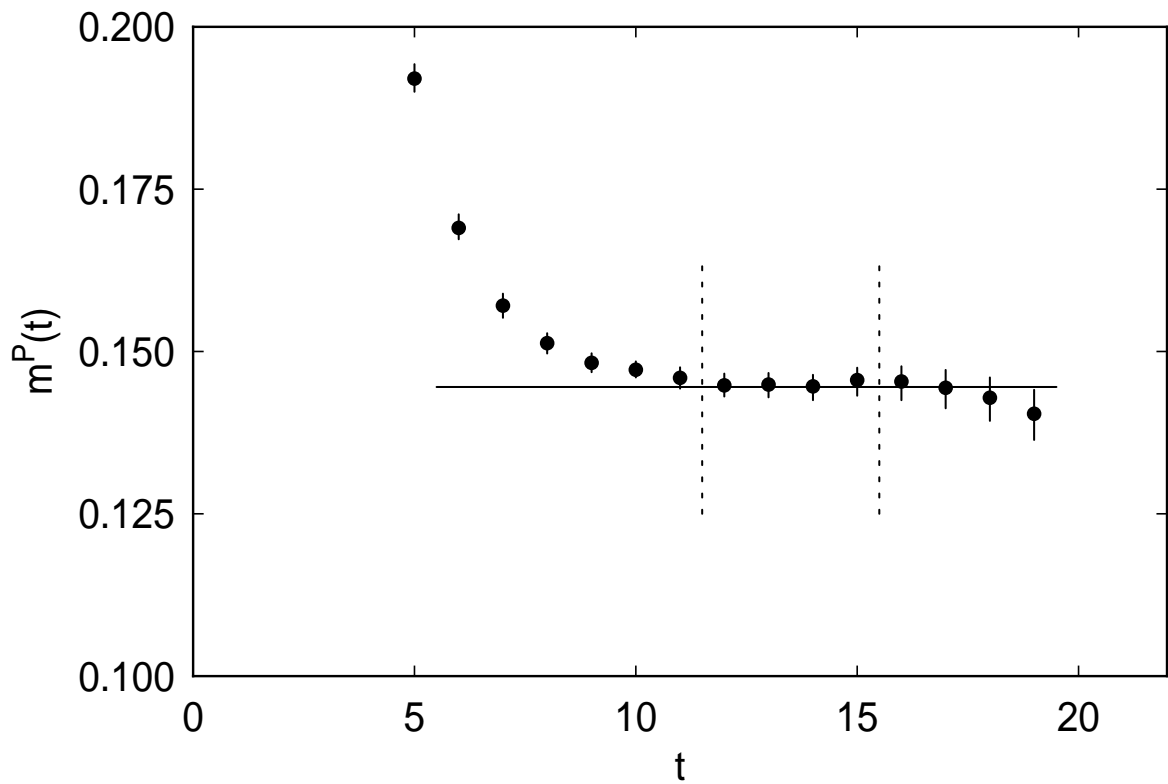


Figure 9: Effective masses and fitted mass for the pseudoscalar propagator  $C_{02}^P(t)$  on the lattice  $30 \times 32^2 \times 40$  at  $\beta = 6.17$  and  $k = 0.1532$

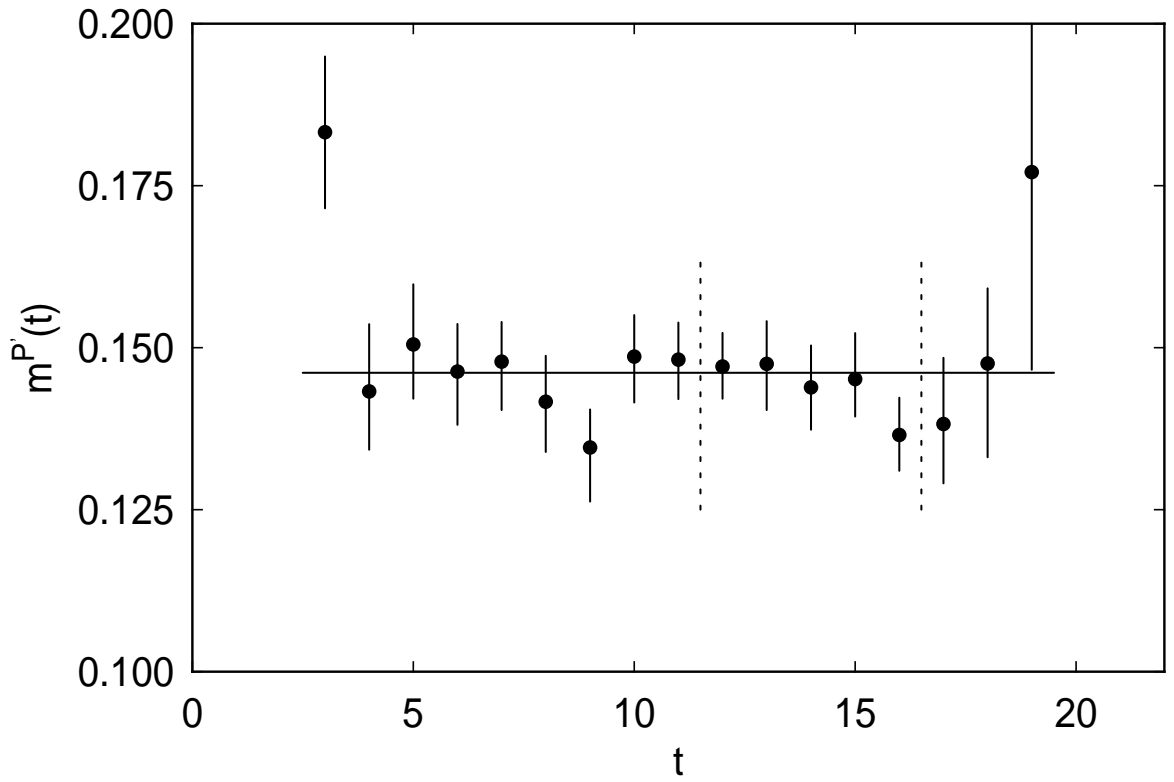


Figure 10: Effective masses and fitted mass for the axial vector propagator  $C_{02}^A(t)$  on the lattice  $30 \times 32^2 \times 40$  at  $\beta = 6.17$  and  $k = 0.1532$

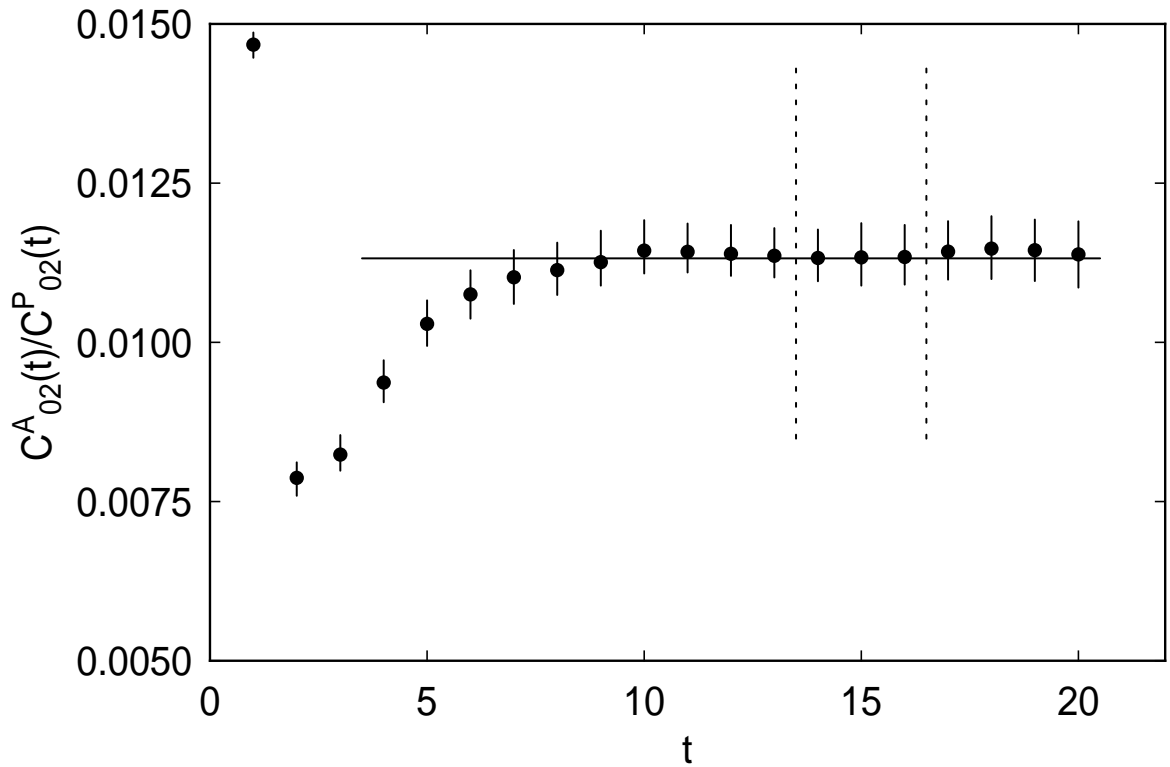


Figure 11: The propagator ratio  $C_{02}^A(t)/C_{02}^P(t)$  and a fit to its large  $t$  plateau on the lattice  $30 \times 32^2 \times 40$  at  $\beta = 6.17$  and  $k = 0.1532$

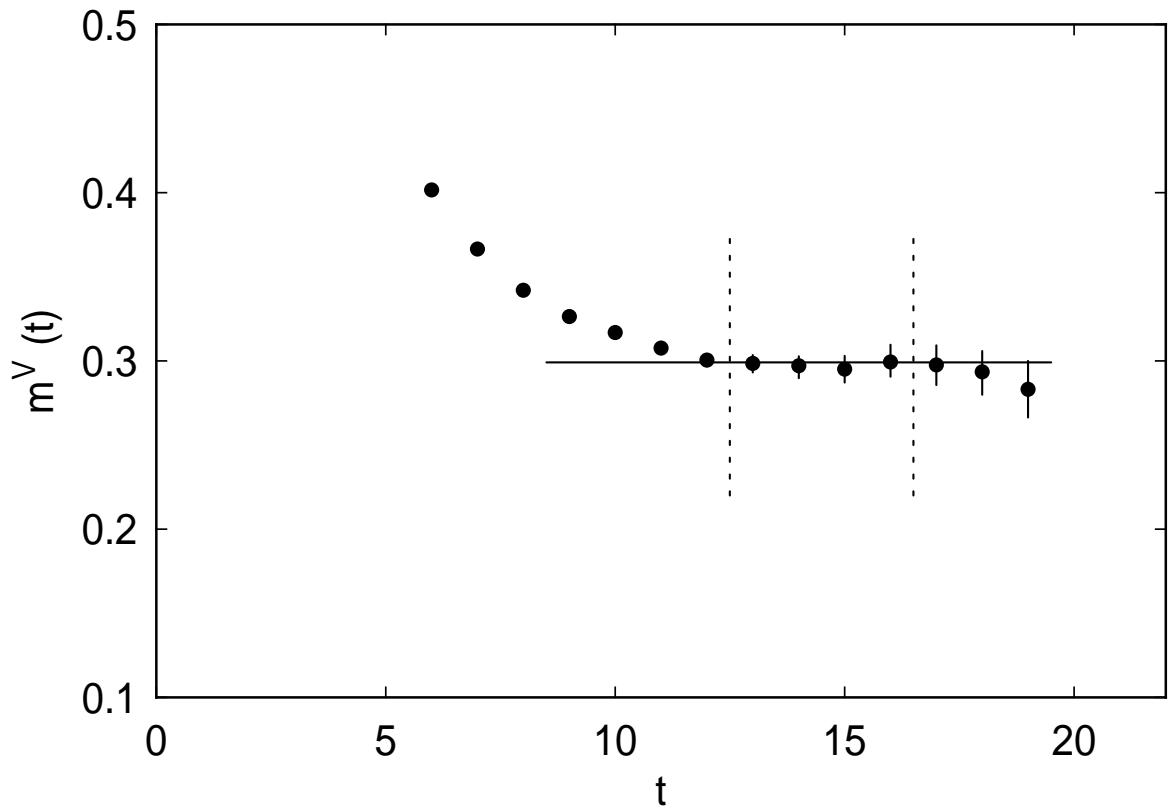


Figure 12: Effective masses and fitted mass for the vector propagator  $C_{02}^V(t)$  on the lattice  $30 \times 32^2 \times 40$  at  $\beta = 6.17$  and  $k = 0.1532$

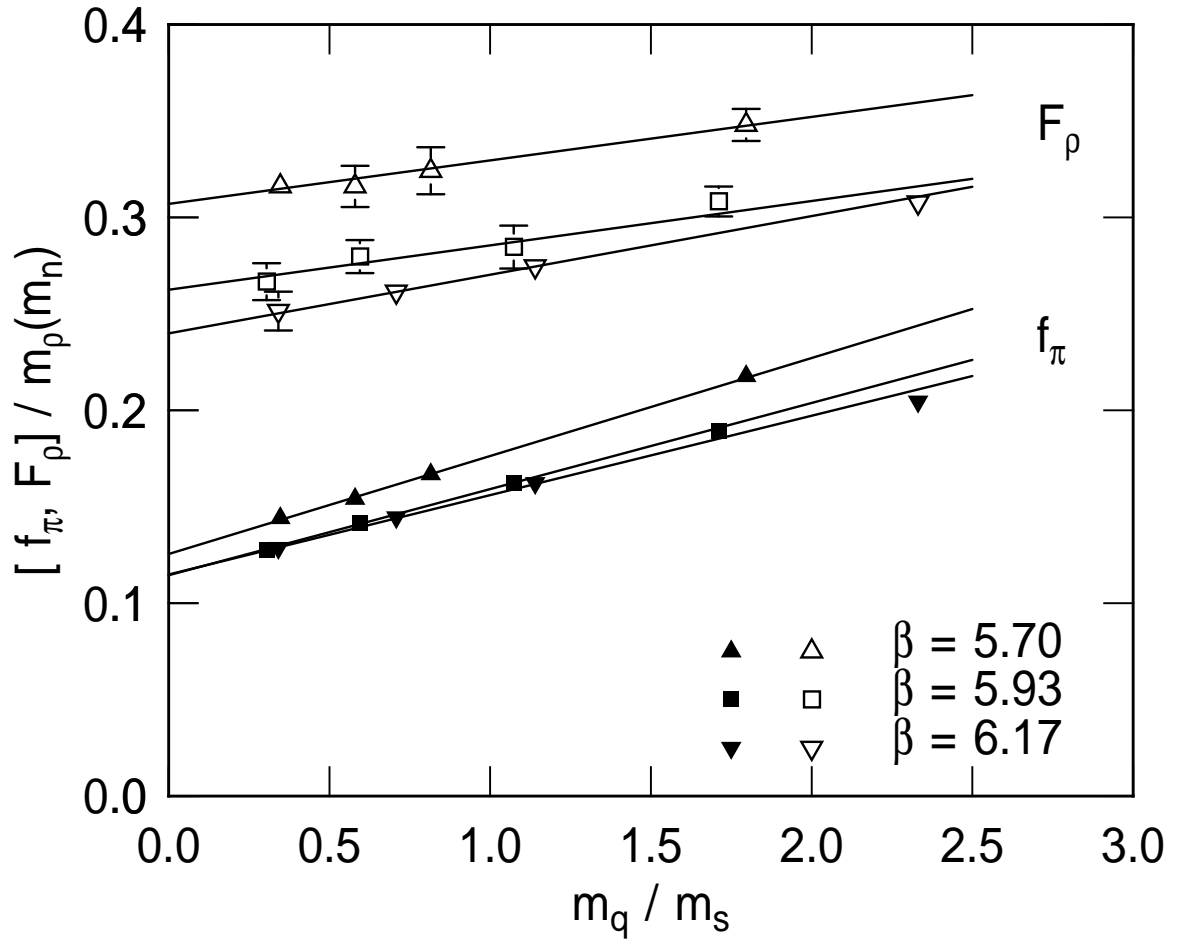


Figure 13: The decay constants  $F_\rho$  and  $f_\pi$ , with perturbative renormalization, in units of the central value of the physical rho mass  $m_\rho(m_n)$ , as functions of the quark mass  $m_q$ , in units of the central value of the strange quark mass  $m_s$ .

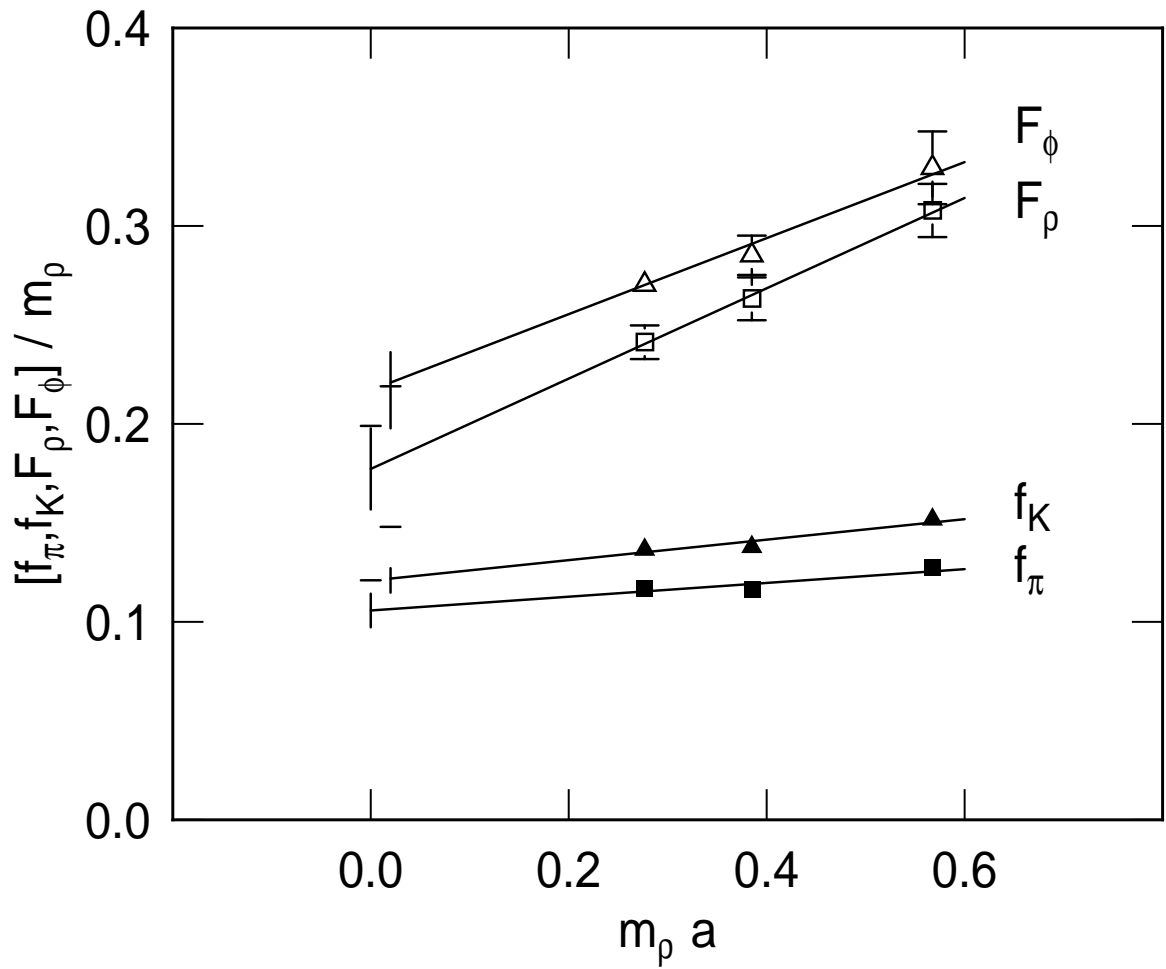


Figure 14: Perturbatively renormalized decay constants as functions of the lattice spacing  $a$ , in units of  $1/m_\rho$ . The error bars near zero lattice spacing are uncertainties in the extrapolated ratios, and the horizontal lines represent experimentally observed values.